SURFACE CHARACTERIZATION BY SINGLE-ATOM MASS SPECTROSCOPY*

Author: **J. A. Panitz**
Sandia Laboratories
Albuquerque, New Mexico

TABLE OF CONTENTS

---

*The author's research was supported by the United States Energy Research and Development Administration.

INTRODUCTION

The atom-probe, imaging field-desorption mass spectrometer, and related techniques (the techniques of *single-atom mass spectroscopies,* or SAMS) occupy a unique place among the methods currently available for surface characterization. Unlike the more conventional electron spectroscopy techniques (Auger, appearance potential, and photoelectron), they are truly surface-sensitive, sampling the constituent species of only the first atomic layer, and since they employ mass-spectrometric means for species identification, they can directly detect all surface species, including hydrogen. Whereas surface structure can only be determined on a gross average scale by diffraction methods, single-atom spectroscopy, incorporating the magnification advantage of the field-ion microscope,[1] can determine the location of individual surface species and detail (on an atomic scale) the extent of localized lattice imperfections. Since such techniques can controllably remove each atom layer of a specimen to expose the one underneath, depth profiling of surface species can be achieved with a resolution unequaled by any other method. Moreover, since species abundance can usually be determined by direct counting of detected species, only detection efficiency (an experimentally determinable parameter), and not theoretical estimates of cross sections or matrix contributions, will determine compositional accuracy. As a result, the single-atom spectroscopy can provide a more quantitative picture of surface and near-surface composition and structure than previously available.

With such obvious advantages, it is curious that single-atom spectroscopy techniques have not been extensively used for surface and near-surface characterization. Certainly, the small specimen dimensions and the possible perturbing influence of the high surface electric field can limit the applicability of these techniques. But practical restrictions imposed by the specimen on the type of problem that can be investigated are not overly severe. For example, the materials that can be successfully examined are not limited to those which can survive the field-ion imaging process, since single-atom spectroscopy can analyze (or even directly observe) the species formed when the substrate field evaporates,[2,3] often at fields *well below* those required for ion imaging. Likewise, adsorbates that are invisible in the field-ion image or indistinguishable from displaced substrate atoms, or that desorb at fields lower than those required for imaging, can be observed and identified, providing a possible means for locating individual binding sites. The usual specimen size (5 to 50 nm) and shape, although preventing examination of macroscopic samples, is an advantage, because it assures simultaneous observation of many individual single-crystal planes, thereby revealing crystallographic dependences without the necessity of changing the specimen. In addition, the large surface-to-volume ratio of the typical specimen is a close approximation to that of commercial catalyst granules,[4] whose small size prevents direct examination by more conventional surface-sensitive techniques. Of course, the high surface field (and resulting field stress, often as large as 450 kg/mm^2) is not a small perturbation, and therefore its effects must be considered. For example, in determinations of substrate composition, field effects are important because they can influence species abundance, encourage the formation of unusual metal-metal and metal-gas complexes, or promote the dissociation of normally stable species. For adsorption studies, field migration is an additional complication,[5-7] since it can noticeably affect crystallographic distributions.

Although high-field effects may limit, to some extent, the applicability of single-atom mass spectroscopy, they cannot be responsible for the general lack of impact that these powerful techniques have had outside of the field-ion community. Practically (in this author's opinion), the situation stems from the limited number of studies of general interest undertaken with these techniques. As we shall see, aside from very few metallurgical investigations (and even fewer related to adsorbate interactions), the primary use of single-atom mass spectroscopy has been in examinations of processes uniquely associated with the high fields of the field-ion microscope. This, of course, was one of the goals of the atom-probe[6] (the first single-atom mass spectroscopy), and, in retrospect, this goal has been admirably achieved; not only has the nature of controversial anomalous image spots in field-ion micrographs been determined, but an entirely new picture of the ion-imaging process has emerged. However, now, almost 10 years later, the obvious potential of the atom-probe to solve a much wider range of problems[6] has still not been realized.

It is the purpose of this paper to present the atom-probe and subsequent techniques to an audience with broad interests, hopefully demonstrating, at least by inference, that their very unique capabilities can be applied to many surface-related problems. Since any appreciation of SAMS will necessarily require an understanding of experimental limitations, and since the major portion of the single-atom literature deals with experimental techniques, experimental considerations will be discussed in some detail. In Sections II to V, the general problems of species identification, mass resolution, and ion detection will be presented, followed by a brief description of atom-probe-related instruments in Sections VI and VII. In Section VIII, atom-probe metallurgical investigations will be discussed, and in Section IX, a synopsis of results directly related to high-field surface processes will be presented. Finally, in Sections X and XI, the new field-desorption techniques will be presented, and in Section XII, a discussion of their results. Hopefully, this approach will convey the strengths and weaknesses of single-atom mass spectroscopy. Possibly, it will demonstrate that such techniques can provide a unique and beneficial way of looking at the surface and near-surface region of many materials. Certainly, it will suggest that single-atom spectroscopy can provide a wealth of information, ranging from observations of basic adsorbate-substrate interactions to routine compositional profiles in those instances where the detection sensitivity of more conventional methods is inadequate. Currently, less than six laboratories throughout the world are involved in single-atom mass-spectrometric investigations. That number must necessarily increase as the power and flexibility of these techniques are appreciated.

I. THE ATOM-PROBE FIELD-ION MICROSCOPE

The atom-probe concept was suggested by Müller[8] in 1967 as a means of identifying the surface species that produce individual image spots on the screen of a field-ion microscope. The method proposed was as elegantly simple, at least in principle, as the ion microscope itself: use the ion image to visually select an atomically resolved region of the surface for observation, then field-evaporate the specimen in a controlled fashion to provide surface species from the region (as positive ions) for analysis in a mass spectrometer. By restricting the acceptance angle of the spectrometer with an aperture, or "probe hole", a surface region limited in extent to several angstroms could be analyzed, and by moving the specimen with respect to the probe hole, any selected portion of the entire ion image could be examined. Of course, probe-hole field-ion spectroscopy was not new in 1967, having been used previously[9,10] to examine the species produced by field ionization of externally supplied gas above the surface or by slow field evaporation of the surface.[10] What was unique with the atom-probe was the sensitivity and flexibility to examine a small number of species from a *preselected* region of the surface.

In principle, one image spot, and therefore one surface species, can be analyzed, but in practice, a small region of the surface, containing several image spots, is usually examined. Since the number of species detected under such conditions is very small, repetitive examinations of the region must usually be made to insure adequate statistics. However, the necessity of repeatedly examining the region can impose severe practical constraints on the type of information that can be obtained. For example, if surface composition is desired, the destructive nature of the examination will force each succeeding observation to be made of a newly exposed surface layer, corresponding to successively deeper penetration into the specimen. As a result, what one obtains is not the composition of the first layer within the region, but rather the composition of the region averaged over a depth within the specimen, determined by the number of identical species needed to obtain adequate statistics. Statistical considerations also determine the effective depth resolution when using the atom-probe to obtain depth profiles of species within a selected region. Although species within one atomic layer can be identified (and therefore, in principle, depth profiles with monolayer resolution are possible), statistical reliability requires the examination of many identical species, usually corresponding to the constituents of several layers, limiting depth resolution to several angstroms. Moreover, statistical considerations also apply when weakly bound adsorbates are chosen for examination, although they can be successively adsorbed and then desorbed from a region without changing the substrate. For such experiments, the number of successive observations required to insure statistical reliability will depend on the probability of detecting an adsorbate within the region being examined. That is, the number of observations will be inversely proportional to adsorbate coverage, with the success of the entire experimental sequence dependent upon maintaining identical surface conditions between observations.

II. THE TIME-OF-FLIGHT ATOM-PROBE

Although any mass spectrometer capable of single-ion detection can be used for atom-probe analysis, time-of-flight (TOF) instruments are particularly attractive, since they are generally simple to construct, allow a complete mass spectrum to be obtained within a very short time, and maximize signal-to-noise ratio because of their ability to precisely time-correlate the ionization event with subsequent species detection. For these reasons, the first atom probe[8,12,13] (Figure 1A) and essentially all current instruments are TOF devices, in which species identification is obtained by measuring the flight time of ions of well-defined kinetic energy over a known drift distance. The essentially monoenergetic nature of the ions and their highly localized point of origin in space combine to provide good mass resolution in TOF instruments of modest dimensions and complexity.

It is beyond the scope of this paper to discuss the details of atom-probe instrumentation, although improvements in design have significantly affected instrument performance and constitute a major portion of the atom-probe literature. Instead, the interested reader is referred to several previous reviews[14-17] and reports of completed instruments,[15-22] as well as to descriptions of specimen manipulators,[18,23-26] electrostatic lens[15,27,28] and deflection[29,30] systems, image enhancers,[27,31] single-ion detectors,[32,33] and electronic counters[25,34] and digital timers[35,36] for travel-time measurements. Although the list of instrument-related papers seems formidable, the actual instrumentation needed for a SAMS study is not more complicated than that required for LEED or Auger analysis. Basically, a manipulator providing suitable movement, cryogenic cooling, high-voltage DC biasing, and nanosecond high-voltage pulse transmission to the specimen is the most demanding and unique feature of the instrumentation. In general, any manipulator providing these functions will suffice, but in practice, unless it is carefully designed, problems with the specimen potential may occur, resulting in poor species selection, identification, detection, and mass resolution. Since a knowledge of these factors is crucial for interpreting any SAMS experiment, they will now be discussed in some detail.

The desorption process in the TOF atom-probe is initiated by applying a short-duration, high-voltage positive pulse of amplitude P to the specimen, prebiased to a DC potential V (Figure 1B). The resulting ions, upon emerging from a closely spaced counter electrode at ground potential, have acquired their final kinetic energy and travel with constant velocity (in a field-free "drift" region) to a detector having single-ion sensitivity. Each species is identified by its mass-to-charge ratio (m/n), obtained by equating its kinetic and potential energies in the drift region,

$$\frac{1}{2}mv^2 = qV_T = neV_T$$

and realizing that the ion's travel time, T, in the drift region is just the length of the region, d, divided by the ion's velocity, ν. That is,

$$m/n = \frac{2e}{d^2} V_T T^2 \qquad (1)$$

where e is the electronic charge, n the charge state of the ion, and the total specimen potential, V_T, the sum of the DC bias and the pulse amplitude. Since the pulse amplitude cannot be directly measured at the surface of the specimen, the actual pulse amplitude that initiates desorption is expressed as αP, where P is the amplitude of the pulse at the pulse generator termination, and α is a calibration parameter called the "pulse factor." The travel time of each ion is obtained by measuring the time between the rise of the desorption pulse and the rise of the detector signal produced by the ion's arrival. However, propagation delays in the measuring equipment and the unknown instant of species desorption during the desorption pulse can introduce a timing error, δ, called the "time delay." If α and δ are constants, or if they vary slowly during the course of an experiment, it can be shown[37] that

$$m/n = \frac{2e}{D^2} (V + \alpha P) (T + \delta)^2 \qquad (2)$$

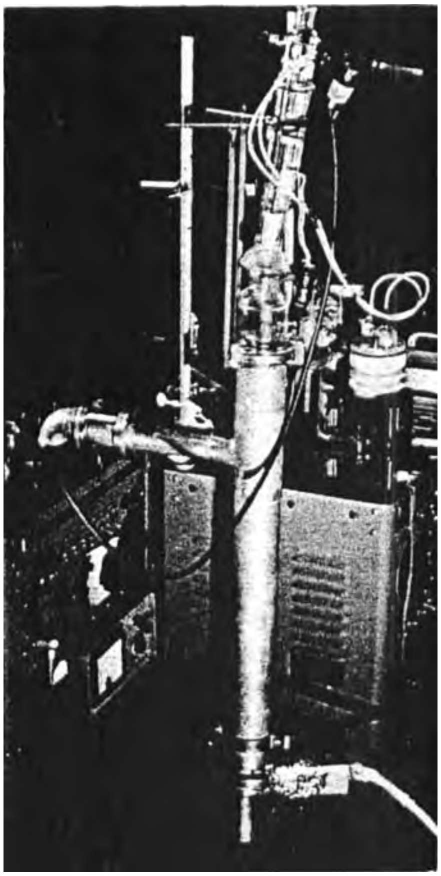

FIGURE 1A. The original atom-probe field-ion microscope. The glass specimen chamber is uppermost, with a spherical grease joint providing specimen movement. The separately pumped drift tube is 1 m long.

with calibration procedures[37-39] used to determine α and δ. Since n, the ion's charge state, can be estimated from field-evaporation theory[40] or is known from experience, mass determinations can be made. Provided that α and δ are carefully determined, an unknown species can be identified within one or two atomic mass units.

III. MASS RESOLUTION OF THE TIME-OF-FLIGHT ATOM-PROBE

The mass resolution of the simple TOF atom-probe is limited by the observed spread in the travel time of identical species. In theory, a constant desorption field is established by the desorption pulse, so that a time spread in the arrival of identical substrate species, equal to the width of the desorption pulse, would be expected.

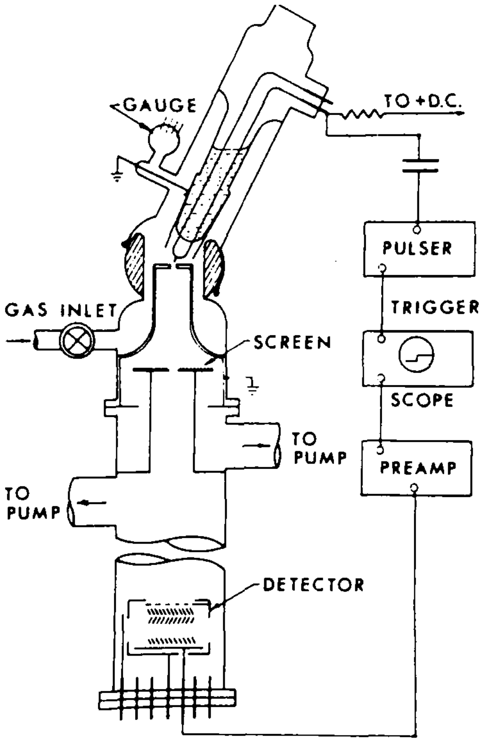

FIGURE 1B. Schematic drawing of the first atom-probe. In newer instruments, high-vacuum specimen manipulators are used, and the fluorescent screen is usually replaced by a CEMA image enhancer containing the probe hole.

This assumes, of course, that the number of identical species capable of field-desorbing is unlimited. If the number of species is limited, either by coverage for an adsorbate, or by a small lattice concentration, or by a reduction in surface field (caused by an increase in specimen radius, resulting from field evaporation of the lattice), a proportionately smaller time spread would be observed. However, regardless of the time spread, the energy of each identical species should be the same, provided that the specimen potential during desorption remained constant and that no surface process introduced an energy loss. In practice, energy measurements[27] of identical field-evaporated species show an energy spread of several hundred eV. Since the spread is too small to be explained by losses due to surface plasmon excitation,[41,42] it is concluded[27] that the desorption pulse does not actually have a constant amplitude, but that its amplitude changes with time during the desorption process. It is the time variation of the pulse amplitude, coupled with a probability for desorption at any point in time during the pulse, which will determine the observed spread in ion energy. However, a time-varying pulse amplitude would additionally lead to an m/n-dependent energy spread, since ions with a small m/n would travel more quickly through the acceleration region than ions with a large m/n, and would, therefore, experience less of the total time variation in the pulse amplitude.[43] This m/n dependence is observed,[44] with several authors attempting to confirm its origin[45,46] by predicting its magnitude from a solution of the equation of motion of ions accelerating near the specimen in a time-varying electric field. However, since the actual time-dependent pulse shape is unknown, the results of such calculations are somewhat academic, although a variation of the calculation (used to estimate a pulse shape from the observed energy spread) can be useful. Still another calculation[47] assumes a pulse shape and then predicts the shape (and therefore time-width) of a substrate mass peak in the TOF atom-probe. Field evaporation for the duration of the pulse is assumed, with a rate exponentially dependent on the instantaneous specimen potential (electric field). Unfortunately, the calculation does not include the effect of the instrument response function (the detection-system characteristic), and therefore cannot accurately predict an observed peak shape, but it can indicate trends for different desorption pulse characteristics.

The m/n-dependent energy spread associated with the detected species also affects unknown-species identification, since the derivation of Equation 2 assumed a time-invariant pulse amplitude. For the purposes of species identification, the time-varying pulse amplitude can be treated by assuming a time-dependent pulse factor, $\alpha(t)$, or, equivalently, a pulse factor that is a function of m/n. Since $\alpha(m/n)$ is a slowly varying function (calibrations assuming that α is a constant identify species with reasonable accuracy over the entire mass range), α can be treated as a constant, at least over small regions of the mass range. Practically, this means that a single-species calibration procedure[31-33] should always be used, with the m/n of the calibration species as close as possible to that expected for the unknown species, in order to maximize calibration accuracy.

Fortunately, the problems associated with the spread in ion energy can be minimized by an instrument modification of relatively minimal complexity,[43] or they can be eliminated entirely by Müller and Krishnaswamy's[48] recent clever adaptation of a Poschenrieder design[49] that can achieve isochronal arrival for identical species having an energy spread of several hundred eV. With such an energy-focused instrument, (Figure 2) time (and therefore mass) resolution is vastly improved, and unidentifiable "artifact" signals are essentially eliminated. $\Delta M/M = 1/1000$ is easily achieved in practice,[48] with greater mass resolution essentially limited only by the duration of the desorption event itself. To minimize this time for all species, it is desirable to use a pulse having an initial voltage overshoot of minimal duration, and then to limit (by careful adjustment of the specimen bias) the desorption process to the temporal duration of the overshoot.[27] Obviously, the amplitude of the overshot must be within the energy-compensation ability of the associated spectrometer. Figure 3 is a histogram showing the resolved isotopes of molybdenum,[50] obtained with the energy-focused TOF atom-probe.

It should be emphasized, however, that for many analytic purposes high mass resolution is not needed, so that the use of an energy-focused instrument is unnecessary. The uncompensated TOF atom probe can easily achieve a resolution[51] of $\Delta M/M = 1/50$, and if care is used in measuring travel times and in obtaining adequate statistics, $\Delta M/M = 1/180$ can be obtained. With such resolution, the isotopes of molybdenum can also be resolved. This is shown in Figure 4 and Table 1, where Seidman[52] has used a conventional atom-probe[22] incorporating a 1.00-m drift distance to obtain the required resolution.

IV. AIMING THE ATOM-PROBE

As was mentioned earlier, atom-probe studies have not actually concentrated on the identification of single preselected species, but rather on the species present within a small region of the surface. The reason, aside from the poor statistics inherent in atom-by-atom analysis, is an experimental difficulty, i.e., aiming, which can directly affect, to some extent, all atom-probe measurements as well as the interpretation of experimental results. *Aiming the atom-probe* refers simply to the ability to unambiguously detect a *single, preselected* surface species. In principle, the local evaporation rate in the region being examined can be controlled so that only one atomic layer will be removed for each pulse applied to the specimen.

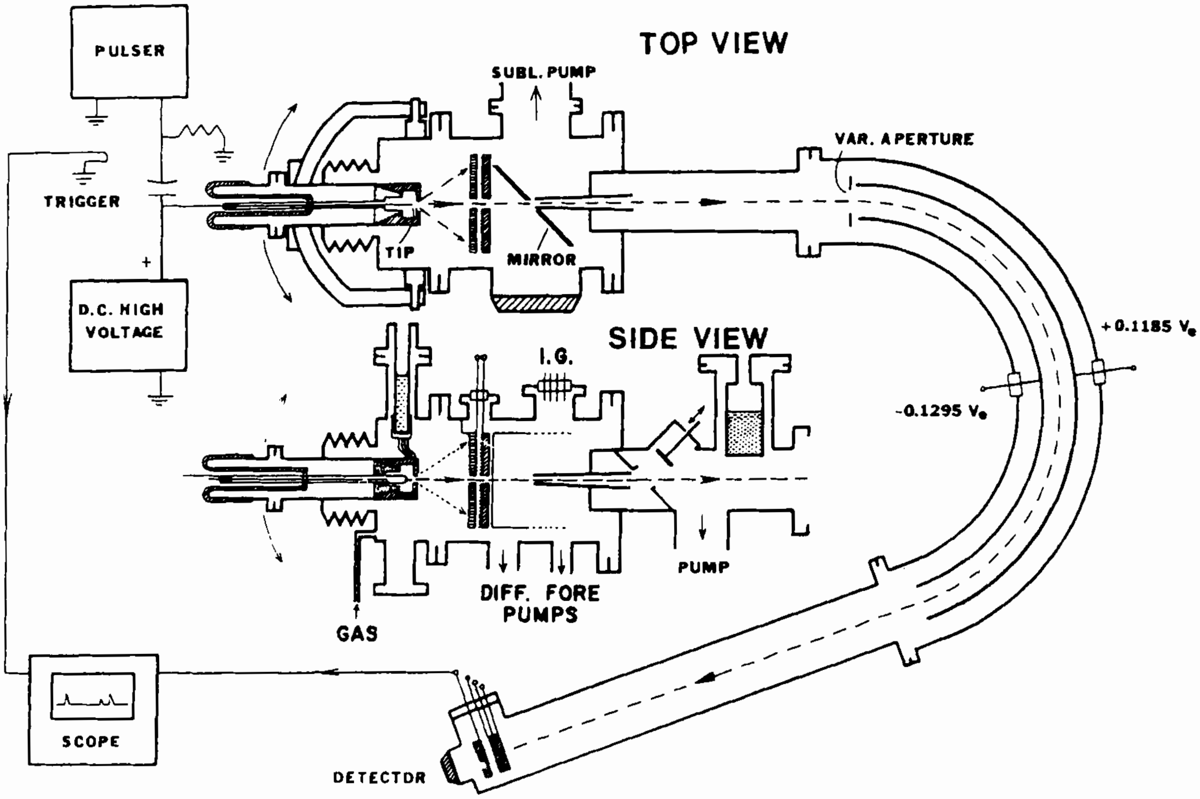

FIGURE 2. The energy-focused TOF atom-probe. Isochronal arrival at a detector is achieved for all field-desorbed species, regardless of any energy deficit introduced by the evaporation pulse. (Courtesy of Professor E. W. Müller, The Pennsylvania State University.)

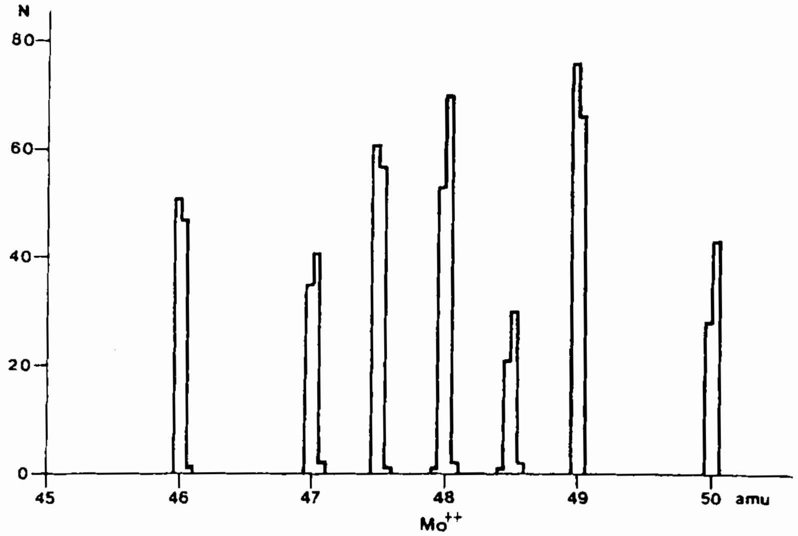

FIGURE 3. Molybdenum-abundance histogram obtained with a TOF atom-probe incorporating Poschenrieder energy compensation. (Histogram courtesy of Professor E. W. Müller, The Pennsylvania State University.)

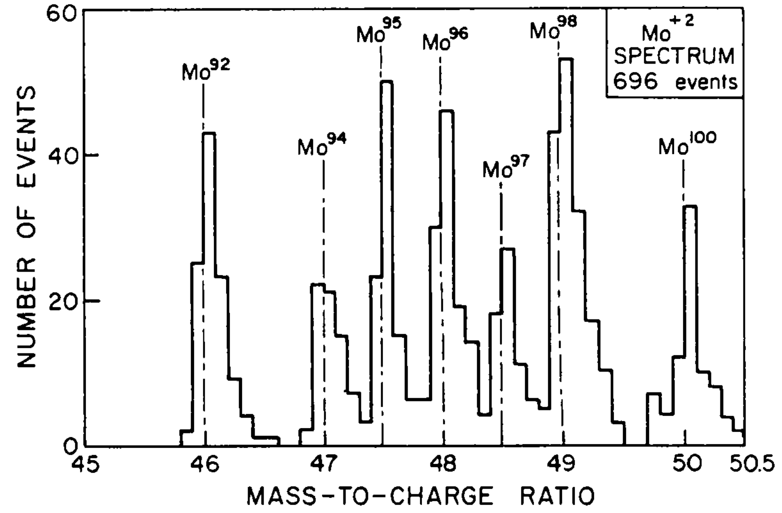

FIGURE 4. Molybdenum-abundance histogram obtained with a TOF atom-probe employing no energy compensation. (Histogram courtesy of Professor D. N. Seidman, T. M. Hall, and A. Wagner, Cornell University.)

TABLE 1

Comparison of the Experimental Mo^{2+} Isotopic Abundances Calculated from Figure 4*

Isotope	AMU range	Number of atoms†	Experimental percentage	Actual percentage
Mo^{92}	45.8–46.6	108	15.5 ± 1.5	15.84
Mo^{94}	46.8–47.4	70	10.1 ± 1.2	9.04
Mo^{95}	47.4–47.9	100	14.4 ± 1.4	15.72
Mo^{96}	47.9–48.4	113	16.2 ± 1.5	16.53
Mo^{97}	48.4–48.9	67	9.6 ± 1.2	9.46
Mo^{98}	48.9–49.5	158	22.7 ± 1.8	23.78
Mo^{100}	49.7–50.5	80	11.5 ± 1.3	9.63

*Courtesy of Professor D. N. Seidman, T. M. Hall, and A. Wagner, Cornell University.

†Total number of Mo^{2+} ions is 696.

As a result, if the probe hole diameter is made equal to the selected ion-image spot diameter, and if a single mass peak is observed after pulsing, a single surface species will have been detected. The question is whether the detected ion corresponds to the surface species whose ion image was placed over the probe hole or to another species some distance away. It was recognized soon after the introduction of the atom-probe[13,18,53] that, in fact, the trajectory of a surface species did not usually coincide with that of the corresponding imaging gas ions used for aiming, resulting in an aiming error that depended on the crystallographic region of the specific material being examined. Although a suggested experiment[13] was independently performed[18] to determine the magnitude of the effect, it was recognized that a complete characterization of the aiming effect could only be provided by a direct comparison of the ion image with the image produced by the desorbed species.[13] Recently, this has been accomplished[54] (Figure 5). However, the crystallographic complexity of the aiming correction, and perhaps the realization that statistical reliability demands more than the identification of one species, has led investigators to minimize aiming difficulties by

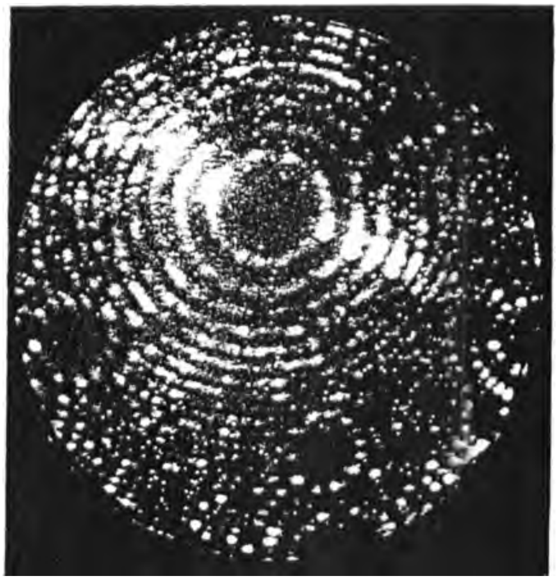

FIGURE 5. Helium-ion image of tungsten surface at 30 K prior to evaporation, with W^{3+} species (resulting from one 20-ns evaporation event) superimposed.

increasing probe-hole size. Practically, several species are examined at a time, so that aiming for a surface *region*, rather than for the location of a single species, becomes important. In addition to making aiming easier, regional examinations provide more species for analysis, thereby improving statistics in each desorption event.

V. SINGLE-ION DETECTION

The success of single-atom spectroscopies is directly related to their ability to detect individual ions with high efficiency. In fact, the discussion of atom-probe aiming assumed that all ions that traveled through the probe hole into the spectrometer would be detected. Otherwise, even the idealized atom-probe experiment designed to determine the identity of a single, preselected surface species would be impossible to achieve. Although many single-ion detectors are available,[32,33] the Chevron-CEMA[55] has been extensively used for atom-probe studies because of its low noise, high gain, minimal transit time and its unique ability to image the detected species with excellent spatial resolution. Since the CEMA is of such importance to all single-atom spectroscopes, it is worthwhile to briefly discuss its characteristics.

The Chevron-CEMA is composed of two microchannel plates or channel electron multiplier arrays (CEMAs) in tandem; each plate is approximately 1 mm thick and composed of millions of individual electron multipliers, usually spaced on 50-μm centers in a regular geometric array. Each multipler, a glass capillary 37μm in diameter and lined with a secondary-electron-emission coating, is inclined normal with respect to the plate, so that an ion arriving at any angle to the CEMA surface will strike a capillary wall and release secondary electrons. A potential difference applied to a conductive layer on the parallel faces of each CEMA plate accelerates the electrons, causing them to strike the channel wall and initiate an electron cascade. The resulting multiplication produces gains of 10^3 to 10^4 before ion feedback (produced by electron-stimulated desorption of species adsorbed on the channel walls) increases background noise to unacceptable levels. Placing two plates in tandem (Chevron-CEMA) permits each to operate at a gain sufficient to minimize ion feedback while producing an overall gain of 10^6 to 10^7. The position of electrons emerging from the second plate, corresponding to the position of ions striking the first plate, can be observed by accelerating the electrons to a phosphor screen. The position of individual ion impacts can therefore be observed (and photographed), or the charge deposited on the phosphor screen can be detected as voltage pulses on an oscilloscope, indicating species arrival. Since electron transit times and transit time spread in the Chevron-CEMA are small (<2 ns), the arrival of ions closely spaced in time can be recorded.

In the past, the areal detection efficiency of a CEMA has been questioned, since it would seem that ion detection is possible only within each channel. Those ions which strike between channels might be expected to go undetected, resulting in an areal detection efficiency determined by the ratio of channel-to-interchannel areas,[56] ≈50% for most CEMAs. Practically, this would mean that only 50% of the ions striking the detector would produce signals, so that a single, preselected surface species (assuming perfect aiming) would be detected only one half of the time.

Fortunately, a recent study[57] of CEMA areal detection efficiency has shown previous estimates to be too low. If the front surface of the CEMA plate is biased at +22 V, and if its conductive electrodes have a high secondary electron yield, 100% detection efficiency can be approached,[57] since such conditions will maximize the collection of secondary electrons in adjacent channels when a positive ion strikes the area between them. A computer simulation was used to optimize the parameters controlling the collection of secondaries produced in the interchannel area.[57] It was observed that large negative biases on the front CEMA surface can drastically lower secondary collection, so that 50% detection efficiencies may frequently occur in practice.

In order to improve the signal-to-noise ratio of the CEMA (or to discriminate between ions arriving successively in time), the CEMA can be time-gated,[43,58,59] usually by pulsing one surface from a DC bias level to its normal operating potential. The minimum gate time is determined by the product of the plate capacitance-to-ground and the impedance of the pulse generator. Gate times of 8.0 ns can be achieved with a source impedance of 25 Ω,[60] and still shorter gate times appear possible.

VI. THE MAGNETIC ATOM-PROBE

Field-ionization sources have been used with probe-hole, magnetic-sector mass spectrometers for many years[9,10] to analyze the species produced by field ionization of gases, and more recently to provide unique "fingerprints" of sulfo-organic compounds[61] uncomplicated by the many fragment species produced with conventional ion sources. In 1968, a 60° second-order-focusing, magnetic-sector mass spectrometer[11] provided the first reliable observations of surface species produced by low-temperature field evaporation, although detector noise and sensitivity (greatly improved over previous instruments) still limited the minimum number of species that could be observed. However, the mass resolution of the instrument was attractive, as was its ability to identify species produced by DC-field evaporation. As a result, a magentic-sector atom-probe was constructed,[43,62] using a similar spectrometer, but incorporating a Chevron-CEMA detector (with a proximity-focused phosphor screen) to improve single-ion detection sensitivity. In the instrument, a region of a conventional field-ion image is positioned by a specimen manipulator over a probe hole in a CEMA assembly (used to enhance the ion image). The aperture in the CEMA provides entrance to a 60°, second-order-focusing, magnetic-sector lens, which disperses the momentum spectrum on a dual-channel plate (Chevron-CEMA) assembly. The specimen potential (ion energy) is kept low, with the required desorption field established by a large negative potential applied to a counter electrode. The resulting mass resolution is high, with $\Delta M/M \cong 1/2000$. Only a portion of the entire mass range can be observed on the detector at one time, because of the sector-field and the Chevron-CEMA dimensions, but, in principle, an instrument could be designed in which the entire mass range (1 to 200 amu) could be displayed simultaneously.

To improve the signal-to-noise ratio, species detection is correlated to the desorption event, either "in space" by only considering events that would coincide, at the detector, with the location of a calibration spectral line, or "in time" by pulse-evaporating the specimen and coincidentally gating the detector.

Because of its ability to precisely identify species produced by DC or long-duration pulse desorption of the specimen, the magnetic atom-probe can complement the TOF technique, and it may prove to be the only simple way to examine semiconducting materials with high bulk resistivities, since high specimen resistivities can prevent a short-duration pulse from establishing the required desorption field at the specimen surface.

VII. THE 10-cm ATOM-PROBE

It is obvious from the description of the atom-probe that a significant amount of information is lost by the probe-hole technique, since only species that travel through the probe hole will be recorded. An obvious solution is to make the probe hole larger or, preferably, to eliminate it entirely, so that the entire surface will be imaged on the single-particle detector at the end of the drift region. However, to accomplish this, a very short drift distance must be employed, since species will diverge, almost radially, from the specimen upon desorption. This further requires a spherically curved detector (with the specimen placed at its center of curvature) in order to insure nearly identical drift distances for all diverging ions. In practice, a compromise must be reached between lengthening the drift region (to improve mass resolution) and sacrificing imaged area (since a very large spherical Chevron-CEMA is difficult and costly to fabricate). An 11.8-cm drift distance

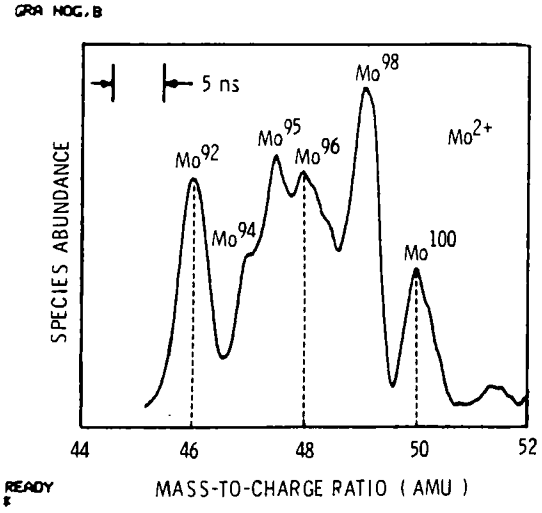

FIGURE 6. A Mo^{2+} isotopic distribution obtained in the 10-cm atom-probe. The evaporation rate was chosen to remove approximately one monolayer; 60 consecutive evaporation events at a fixed specimen potential (V_{DC} = 6.65 kV, V_{pulse} = 1.0 kV) were recorded, using a Tektronix Type 7912 transient digitizer. The mass spectrum resulting from each event was added to the previous spectrum, with the sum of all 60 spectra displayed on a Tektronix Type 4010 graphics terminal and recorded by a Tektronix type 4610 hard-copy unit as shown. Axis and labels were subsequently added. For such spectra, the detector time constant (2.0 ns) and the digitizer amplifier bandwidth (2.0 ns) limit the time and, therefore, mass resolution. Nevertheless, the resolution is comparable to that of a conventional 1-m atom-probe (Figure 4 and Table 1).

with a 7.6-cm-diameter spherically curved (11.8 cm radius) Chevron-CEMA seemed reasonable, and so an instrument was developed by Panitz[63] with these parameters, permitting analysis of approximately 10% of the field-desorbed specimen surface. Although such an instrument had also been considered by Müller,[64] experimental difficulties and an expected low mass resolution discouraged its development.[64] Actually, a mass resolution comparable to that obtained with a conventional atom-probe (Figure 4) can be achieved. This is seen in Figure 6, where the isotopes of molybdenum have been resolved. Obviously, the ability to detect species from many crystallographic regions is an additional advantage. This is particularly true if the species of interest may be removed from the specimen by the first desorption pulse, or if they are only found in highly localized regions of the surface and cannot be recognized in the ion image, so that placement over a probe hole is impossible. An example of the former condition would be species transferred to the specimen surface during the ingenious field-ion contact experiments,[64,65] in which the specimen is made one member of a pair of touching electrodes in order to observe contact damage on an atomic scale. We shall see later that the latter condition (typified by hydrogen adsorption on tungsten) has been obviated by the use of the 10-cm technique.

Localized regional examinations (used to display crystallographic specificity) are desirable, and they are easily accomplished by the use of external, apertured photomultipliers[63] positioned over regions of interest in the ion image, which is displayed on the phosphor screen of the Chevron-CEMA prior to desorption. Since several photomultipliers can be used, several crystallographic regions can be examined simultaneously, but mass resolution is limited by the phosphor rise time (≈ 80 ns), giving $\Delta M/M \cong 1/15$.[63]

VIII. METALLURGICAL INVESTIGATIONS

The utility of the single-atom mass spectroscopy techniques rests in their great sensitivity and in their ability to identify specific, *preselected* surface species. Figure 7 demonstrates their analytic capability by comparison with other surface-sensitive techniques,[66] including Auger electron spectroscopy (AES), ionization spectroscopy (IS), soft X-ray appearance potential spectroscopy (SXAPS), electron spectroscopy for chemical analysis (ESCA), proton-induced X-ray analysis (PIX), and Rutherford backscattering (RBS). With the possible exception of ESCA, only single-atom spectroscopies can detect all surface species, including hydrogen, with excellent elemental identification, but unlike the other techniques, SAMS analysis is destructive. That is, in order to identify surface species with SAMS, the species must be removed from the surface, thereby completely altering (destroying) the characteristics of that surface. Practically, this feature of SAMS analysis places definite constraints on the type of problem that can be investigated. For example, although the other surface-sensitive techniques can continuously follow changes in surface composition during annealing, SAMS (in order to obtain the same information) must perform a series of separate experiments in which identical surfaces, established in each experiment, are first

TECHNIQUES OF SURFACE ANALYSIS

	AES	IS	SXAPS	ESCA	PIX	RBS	SAMS
Elements that can be detected (in principle)	Z>3	Z>1	Z>3	Z>1	Z>3	Z>1	Z>1
Elements that have been detected	Z>3	Z>4[a]	Z>3[a]	Z>1	Z>4	Z>3	Z>1[d]
Elemental identification[b]	VG	E	E	E	VG	G	E
Sensitivity for peak/bkgd • 1 (in monolayers)	~0.02	~0.02	$\lesssim$0.1	~0.02	~0.1	10^{-3}-100	•
Depth probed (in A)	~30	~30	~30	~30	~10^4	~10^4	~1
Chemical (i.e., binding) information[e]	Yes	Yes	Yes	Yes	No	No	No[e]
In principle, results are[c]	Abs	Abs	Abs	Abs	Abs	Abs	Abs
In practice, results are[c]	Rel	Rel	Rel	Rel	Abs	Abs	Abs
Depth distribution	Y/D	Y/D	Y/D	Y/D	Y/D	Yes	Y/D
Complexity of equipment	Med	Med	Low	High	High	High	Med

a - Depends On Element

b - E: Excellent; VG: Very Good; G: Good

c - Rel: Relative; Abs: Absolute

d - Y/D: Yes, but destructive (e.g., sputtering plus analysis)

e - Binding site information only

• - Single-atom detection

FIGURE 7. Comparison of several surface-sensitive techniques (see text). Of those listed, only SAMS (single-atom mass spectroscopy) will destroy the surface during examination. However, the single-atom sensitivity of these techniques and their depth resolution of 10 nm are important assets. (Figure courtesy of R. J. Musket, Sandia Laboratories.)

heated to different annealing temperatures, and then destructively analyzed to determine surface composition. Obviously, the ability to establish identical conditions prior to each observation is a distinct difficulty and will ultimately determine the success of this approach. Fortunately, in many studies (usually of metallurgical interest) this problem is minimized. For example, in the determination of precipitate composition in alloys as a function of aging, many separate precipitate particles are always present, so that a SAMS analysis can be performed on one particle at one time, and (following aging) on another particle at a later time.

The ability of SAMS to identify one atom within a monolayer of atoms provides a detection sensitivity unavailable with other surface-sensitive techniques. Typically, these other techniques require 10^{10} atoms for analysis in order to provide a tolerable signal-to-noise level, whereas SAMS requires only one. Such sensitivity may provide the only way of determining surface impurity concentrations in semiconductors having extremely low dopant levels. Likewise, depth resolution is impressive, making SAMS the only true surface-sensitive technique. Although binding energies are not directly available from SAMS analysis, binding-site information may be obtainable, because of the ability to examine the surface with atomic resolution. Such an ability also permits precise determination of lattice structure and morphology, information that is not available with the other techniques. Unlike the other methods of analysis, SAMS can provide absolute species abundances (by direct counting of detected ions) as well as depth-profiling with monolayer depth resolution.

To date, only the first SAMS technique (the probe-hole TOF atom-probe) has been used in metallurgical investigations. In addition to routine compositional analysis, several of the studies have provided unique and fruitful information concerning the nature of small precipitate particles (< 10 nm), information impossible to obtain by any other method. Such precipitates have important practical consequences, since their size, distribution, and composition within a host matrix can determine its structural integrity. For example, Brenner and Goodman[67] have examined the precipitated nitride phase of the nitriding process used to harden steel surfaces by analyzing the composition of platelets formed in an Fe-3 at.% Mo alloy. The results indicated an average composition, $Fe_3Mo_3N_2$ (having twice the nitrogen content of the postulated equilibrium phase); larger precipitates (10 nm in diameter) consisted of almost pure Mo_3N_2, with some of the molybdenum replaced by iron.

A very complete and beautiful study of copper precipitation in Fe-1.4 at.% Cu alloys was made by Goodman, Brenner and Low,[68] using the field-ion microscope to determine the size and number density of the precipitates, and the atom-probe to determine the composition. For comparison, pure Fe and Cu were also examined in the atom-probe, indicating extensive hydride formation for Fe (FeH and FeH_2) at low partial pressures of hydrogen ($<10^{-9}$ torr), with even more extensive hydriding observed for Cu. Large precipitate particles (>10 nm), obtained after aging the alloy for 40 hr, showed a sharply defined particle-matrix interface, with the almost pure Cu composition of the particle changing to the matrix composition over a distance of less than 1 nm. Particle examination as a function of time showed that, between the first and third hr of aging, composition averaged 50% copper, then increased, and approached 100% copper well after the alloy had reached maximum strength. A thermodynamic argument confirmed the experimentally observed compositions.

Youle, Turner and Ralph[69] examined carbide precipitation in an Fe-V-Mo-C alloy obtained by quenching and tempering, or as the result of isothermal transformation. The precipitates exhibited characteristics of both vanadium and molybdenum carbide, with a mean composition of $(Mo + V)_{1.5}C$ for 15-nm particles, and with an appreciable amount of Fe appearing in the smaller (5 nm), quenched and annealed specimens.

For Fe-Mo-C alloys, Turner and Papazian[70] have observed Mo_2C precipitates after isothermal transformation, whereas Fe-Mo-N alloys gave Mo_2N precipitates, with 10% of the molybdenum replaced by iron after aging. A complementary examination of Fe-C alloys indicated broad-zone (40 nm) carbon segregation in the vicinity of grain boundaries, but there was no indication of preferential segregation of carbon into the grain boundary (at least in monolayer concentrations).

The characteristics of molybdenum carbide precipitates in iron alloys were also described by Turner, Regan and Southon,[25] who found a precipitate composition of $Mo_{1.91}C$ in close agreement with the expected composition, Mo_2C. They also obtained good agreement between the composition of precipitate particles in an alloy steel containing molybdenum and vanadium and that of the original alloy. An unusual observation was the absence of iron in the precipitates, even though iron dominated the composition of the alloy as a whole.

Pre-precipitation clustering in a Ni-13 at.% Ti alloy was mentioned by Turner, Regan and Southon,[71] who presented evidence for the existence of several regions of enhanced titanium concentration, with an overall titanium concentration closely approximating that of the alloy. Mixed molybdenum and vanadium carbide precipitates were also mentioned, as well as the first published atom-probe spectrum of aluminum.

Dunlop and Turner[72] extended the study of carbide precipitation to low-alloy steels containing vanadium and titanium. The composition of platelets (4 to 5 atomic layers thick) by isothermal transformation showed the presence of V, Ti, and C. Larger particles (5 to 6 nm) always indicated a greater titanium concentration than vanadium concentration, even though a lower atomic percentage of titanium existed in the bulk. Such observations suggested that a significant amount of vanadium remained dissolved in the matrix following isothermal transformation. Iron was not observed in larger particles (>20 nm), despite its presence in the bulk. The constituent distribution in larger particles appeared to be random, with no vanadium or titanium seen at the particle edge. After aging for 27 hr at 800°C, carbides of the form $(V_{0.45}Ti_{0.55})C_{0.84}$ were observed. Iron, initially seen in small concentrations, always disappeared during the aging process.

Brenner and McKinney[18] reported that the composition of several dilute alloys (Fe-4.9 at.% Mo, Fe-3.8 at.% Au, Pt-20 at.% Ni, and Fe-1.55 at.% Cu) obtained by the atom-probe were in good agreement with compositions determined by independent chemical means.

In a recent study, Krishnaswamy, McLane and

Müller[73] used the atom-probe to examine the depletion of chromium from stainless-steel surfaces, first reported by Park, Houston and Schreiner[74] from SXAPS studies of macroscopic specimens. The atom-probe study confirmed that chromium depletion (responsible for the corrosion of stainless steels) occurred at elevated temperatures, but indicated depletion times several orders of magnitude lower than those found by Park. This difference was shown to be consistent with the large surface-to-volume ratio of the atom-probe specimens. The authors[73] suggested caution when examining alloys in the atom-probe (specifically after an annealing treatment), since depletion or enrichment could appreciably alter the expected bulk compositions.

The studies above are all of the published TOF atom-probe investigations relevant to material properties, with the possible exception of a study by Brenner and Goodman,[75] reporting experimental confirmation of a theoretically predicted[76] hydride, $BeH(H_2)^+$, and a study by Tsong, Krishnaswamy, McLane and Müller[77] of Pt_3Co, in which the position of the cobalt species ("invisible" in the field-ion image, but "established" by atom-probe analysis[78]) had been questioned.[79]

IX. INVESTIGATIONS OF SURFACE PROCESSES

Two classes of surface processes are of interest to the potential user of single-atom mass spectroscopies. The first is characterized by the high-field phenomena uniquely associated with the ion microscope, and the second is concerned with the zero-field processes encountered in conventional studies of solid surfaces. In order to use the single-atom spectroscopies to characterize processes normally observed at zero field, it is essential to understand the extent to which the high field will perturb the system being investigated. Although studies of high-field phenomena are of great practical importance, they may also be of intrinsic interest, since the high-surface field can cause measurable manifestations of quantum-mechanical tunneling and resonance effects,[80] and may even provide unique insights into the surface density of states[81] and the Fermi surface[82] of common metals.

The first and most obvious effect of the high-surface field is the production of highly ionized substrate species during field desorption. Since compositional analysis with SAMS depends on accurate mass determinations, a knowledge of the charge state of the field-evaporated ions is of practical importance, because the mass of an unknown species cannot be determined independently of its charge. Early atom-probe experiments,[12,23,24,28,83] evaporating a known substrate, indicated highly charged ions, whose abundance was later related to substrate temperature, evaporation rate, and the presence of surface adsorbates.[15,16] Since residual gas will reach the surface and adsorb only at low fields, the observed charge state, in vacuum, will also depend on the field strength,[15] other factors being equal. For the refractory metals (W, Mo, and Ta), three- and even fourfold-charged species are common at cryogenic temperatures, whereas the platinum-like metals (Ir, Pt, and Rh) evaporate as doubly or triply charged ions. Singly and doubly charged species dominated for Au, Ag, Be, and Cu. Although field-evaporation theory could predict the occurrence of doubly charged ions and their temperature dependence,[15] the higher-charge states observed were unexpected, and as yet no satisfactory theory is available that will predict their observed abundance or crystallographic distribution. Fortunately, the observation of many metals and adsorbate-metal systems has provided an extensive catalog of species charge states, permitting accurate mass determinations to be made in situations of practical interest.

A surprising observation made with the TOF atom-probe was the presence of ion-imaging noble-gas atoms adsorbed on the specimen surface[84-87] (even at 80 K, when Van der Waals binding is negligibly small). The effect, interpreted in terms of a field-induced dipole-dipole bond[88] between gas and substrate atom, has led to a complete revision of earlier models of the imaging process in the ion microscope. Later experimental results, localizing the adsorbate to apex positions on the protruding surface atoms,[8,9] indicated that field ionization actually occurs by electron tunneling through the adsorbed noble-gas species, an energetically easier process than direct tunneling into the metal. Based on the atom-probe observations, a quantum-mechanical calculation of the tunneling probability through an adsorbed noble-gas atom has been developed by Nolan and Herman.[90] Obviously, all future theoretical treatments of the field-ionization process must include the influence of these adsorbed species.

A related observation has been the frequent occurrence of metal-noble gas molecular ions,[85,91] whose stability is at least sufficient to prevent dissociation in the acceleration region of the TOF atom-probe. (Dissociation within the acceleration region is detected by the appearance of fragment species having well-defined relative energies.[13]) Initially, a helium-metal ion (helide) was postulated to explain an apparent broadening of tungsten mass peaks when evaporating in helium, since mass resolution did not permit unambiguous identification. Recently, however, high-resolution TOF atom-probe studies have confirmed their existence and show that, for rhodium as well as for tungsten, helide formation is very probable.[27] Further examinations of the tungsten helide species have demonstrated their crystallographic behavior as well as a noticeable temperature dependence.[92] Metal-neon ions (neides) are less frequently seen in TOF investigations; the existence of metal-argon and metal-krypton species has not been confirmed.

Although TOF investigations have not shown appreciable neide abundance, preliminary magnetic atom-probe[62] studies demonstrate that $PdNe^+$ is a dominant species when field-evaporating palladium in the presence of neon and hydrogen. It is not known why a drastically different $PdNe^+$ abundance is measured by the two techniques, although it is tempting to attribute the observation to the different evaporation conditions imposed on the substrate. The TOF instrument uses nanosecond evaporation fields, whereas the magnetic atom probe evaporates the substrate under DC or slow (microsecond) pulse conditions. It is possible that electrons tunneling from field-ionizing neon (occurring with high probability only under slow evaporation conditions) promote $PdNe^+$ formation, either directly by metastable excitation, or indirectly by encouraging hydrogen-assisted catalysis at the surface.[62] However, it is not clear that this is the correct mechannism, since one could argue that electron-induced dissociation of $PdNe^+$ should also occur with high probability. In any event, the observation of different $PdNe^+$ abundances when using two different atom-probe instruments raises a question of critical practical importance: to what extent is the occurrence of any species in a SAMS study the direct result of the magnitude and duration of the desorption field? It is apparent from the previous discussion that metal-gas complexes can form from a field-induced interaction between a substrate atom and an adsorbed species whose very existence on the surface is due to the field. Furthermore, the duration of the field may determine the abundance of a species, in addition to its ability to migrate over the surface. It is expected that the probability for long-range species migration will increase with increasing field duration, suggesting that TOF measurements would be only minimally influenced by long-range migration. However, short-range field-induced migration (a shift in species location from one site to a neighboring site)[93] can also occur, perhaps in extremely short times, so that even TOF measurements could be influenced. As a result, great care will have to be taken if one wishes to use SAMS to obtain the location of individual adsorption sites.

In addition to the formation of metal-gas complexes and field-induced migration, other field effects are also probable. For example, Brenner and McKinney[94] have reported the occurrence of displaced lattice atoms following the adsorption of Co or N_2 at fields above 36 V/nm. Their data suggest that tungsten-gas complexes can be formed, followed by field dissociation (leaving a displaced tungsten atom and a gas species that quickly field-desorbs). Panitz,[95] examining residual-gas adsorption on tungsten at low fields (< 20 V/nm) with the 10-cm atom-probe, found similar species (including those characteristic of the residual gas). Müller, Krishnaswamy and McLane[27,96] investigated CO and N_2 adsorption on various metals and reported dissociation of the molecular species even at 80 K. Their results are particularly important in that field-induced dissociation is indicated (rather than dissociative adsorption), since molecular CO is the most abundant species seen in thermal-desorption measurements at low temperatures. A complete summary of field-desorbed species seen following gas adsorption on various metals (and graphite) has been published by Müller and Tsong.[15] In general, it is possible to observe all conceivable complexes formed by dissocation of the adsorbate or by the permutation of adsorbate and substrate atoms each displaying the range of charge states normally observed for the substrate species alone. Therefore, the complexity of any atom-probe spectrum will depend on the surface conditions prior to desorption. For example, in an ultrahigh-vacuum environment, surface adsorption will be minimized, and atom-probe spectra will become particularly "clean," displaying the substrate species in their various charge states, hydrogen, substrate hydrides, and helium, or possibly helide molecules, if helium was used previously as an imaging gas. Of particular interest is the observation of abundant metal hydrides, since other techniques cannot directly detect their presence on the surface. All materials examined by SAMS have shown hydride formation (often with an abundance equal to the substrate species), and often only as a result of residual hydrogen in the vacuum system.[11,28,68] Since some of the refractory-metal hydrides are not seen at zero field, it is possible that the high-field conditions encourage hydride formation by a mechanism that is not yet understood.

The recognition of field-induced species formation, dissociation, and migration is critically important to any interpretation of a SAMS experiment, but particularly when the techniques are used to examine an adsorption process usually studied by more conventional surface methods at zero field. The temptation is to ignore the presence of the high field and to extrapolate the resulting data to zero field. In metallurgical investigations, the same difficulties exist, although the problem of field-induced migration is usually less critical, since most species of interest are trapped within the lattice and therefore immobilized until an evaporation event removes them from the substrate. However, field-induced corrosion[97] of the substrate may cause additional difficulties by disordering the surface or changing its composition. Practically, a more complete understanding of high-field processes is essential before the single-atom spectroscopies can be used with full confidence; as a result, future work in this area must have very high priority.

X. FIELD-DESORPTION MICROSCOPY

The success of an atom-probe investigation relies primarily on the ability of the detector to record the arrival of each desorbed species. With the advent of the Chevron-CEMA, imaging of the arriving ions in the atom-probe became possible, and a true field-desorption microscope became a reality. For years, the hope of imaging the surface by direct recording of desorbed species has been attractive, with early attempts by Müller and Bahadur[98] and by George[99] (who used a three-stage magnetically focused image intensifier) proving unsuccessful. Realizing the CEMA's sensitivity in atom-probe investigations, Walko and Müller[99] used a single CEMA and an external three-stage image intensifier to obtain the first photographs of individual field-desorbed tungsten atoms (Figure 8). Panitz[63] used a Chevron-CEMA assembly with fiberoptics coupling to record more effectively the desorption images of tungsten in the 10-cm atom-probe.

The desorption image is of interest because it results from the direct detection of surface species and therefore, unlike the gas ion image, records the presence of all species and their relative positions, regardless of their chemical identity. Since each species produces one sharply defined image spot, the desorption micrograph is much sharper than its ion-image counterpart, in which each image spot is produced by the superposition of many thousands of image gas ions, each following a slightly different trajectory. As a result, even desorption micrographs taken at room temperature are sharp, offering the potential of observing surface processes at more elevated temperatures. Unfortunately, the desorption images are noticeably less ordered than the corresponding ion image, even at low temperatures, and therefore they display considerably less substrate symmetry. This "disorder" results primarily from the variation in evaporation rate over the surface; for example, if one surface layer is removed from the (110) plane of tungsten, two layers will evaporate from the (111) region, destroying the regularity observed in the steady-state ion image. Additionally, for very small single-pulse evaporation rates, substrate species will appear to be removed from random locations on the surface, although a superposition of successive desoprtion micrographs will show the expected removal of kink-site atoms, corresponding to the attainment of a stable surface of minimal energy. Obviously, adsorbed species will also be removed during the imaging process, and since hydrogen and helium are known to adsorb freely, the desorption image, even if taken in ultrahigh vacuum, will include their contribution. Since hydrogen can sit in interstitial locations on the surface and even "probe" the three-dimensional structure of the lattice on relatively open planes, its images will further confuse the overall desorption-image symmetry. Obviously, the way

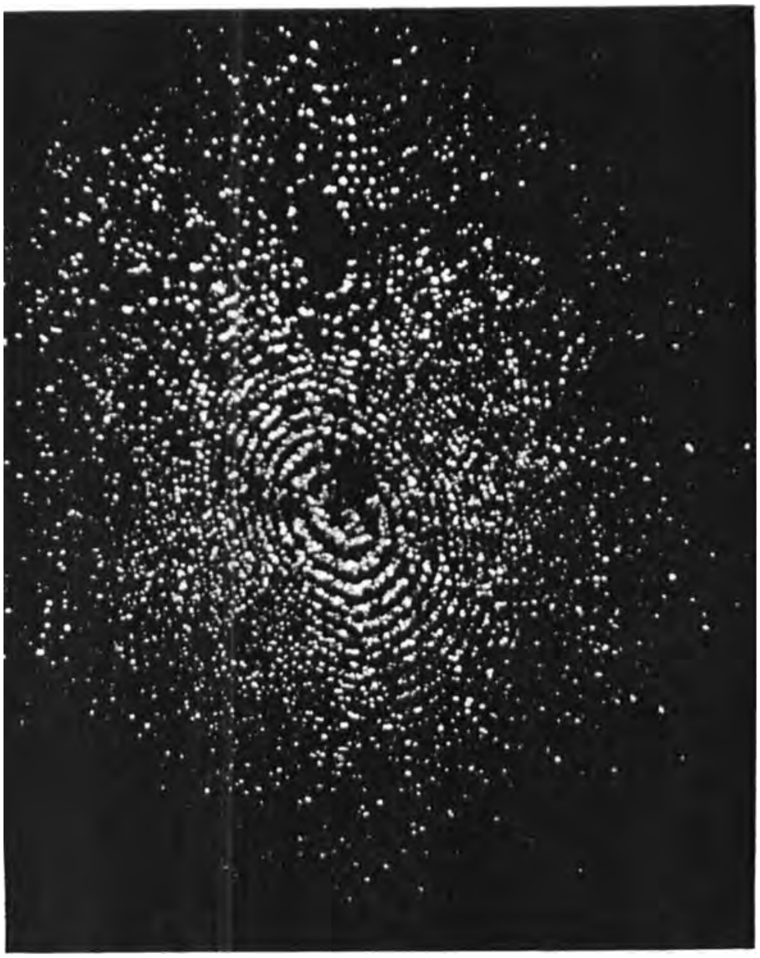

FIGURE 8. Desorption micrograph of tungsten at 78 K. Dark spot (above center of 110 plane) is a detector anomaly. (Micrograph courtesy of Dr. R. J. Walko, The Pennsylvania State University, now at Sandia Laboratories.)

to prevent the interference of overlapping images of various species is to prevent the unwanted species from imaging at the detector. Since each species will take a unique amount of time to reach the detector in a time-of-flight atom-probe, the desired effect can be achieved by time-gating its detector. Although the procedure was considered by Müller and Walko,[43,64] experimental difficulties[64] (and the low mass resolution necessitated by short drift distances) discouraged its development. Independently (and as an obvious extension of the 10-cm atom-probe), Panitz[59] developed a successful time-gating technique, resulting in the first observation of the different species removed from the entire surface of a tungsten specimen during field desorption. Since the method differed from conventional atom-probe microscopy, but relied on the desorption process, it was called *field-desorption mass spectrometry.* However, to distinguish it from Beckey's established technique,[10] it is now called *Imaging Field-Desorption Mass Spectrometry,* or *IFDEMS.*

XI. IMAGING FIELD-DESORPTION MASS SPECTROMETRY

Although related by technique to the atom-probe, imaging field-desorption mass spectrometry provides a different perspective of surface species. Rather than asking for the identity of a single species, or of several species within a small region of the surface, it concentrates on one species, asking for its complete crystallographic distribution on the surface. This distinction is schematically shown in Figure 9, where the result of an atom-probe experiment (a detector signal

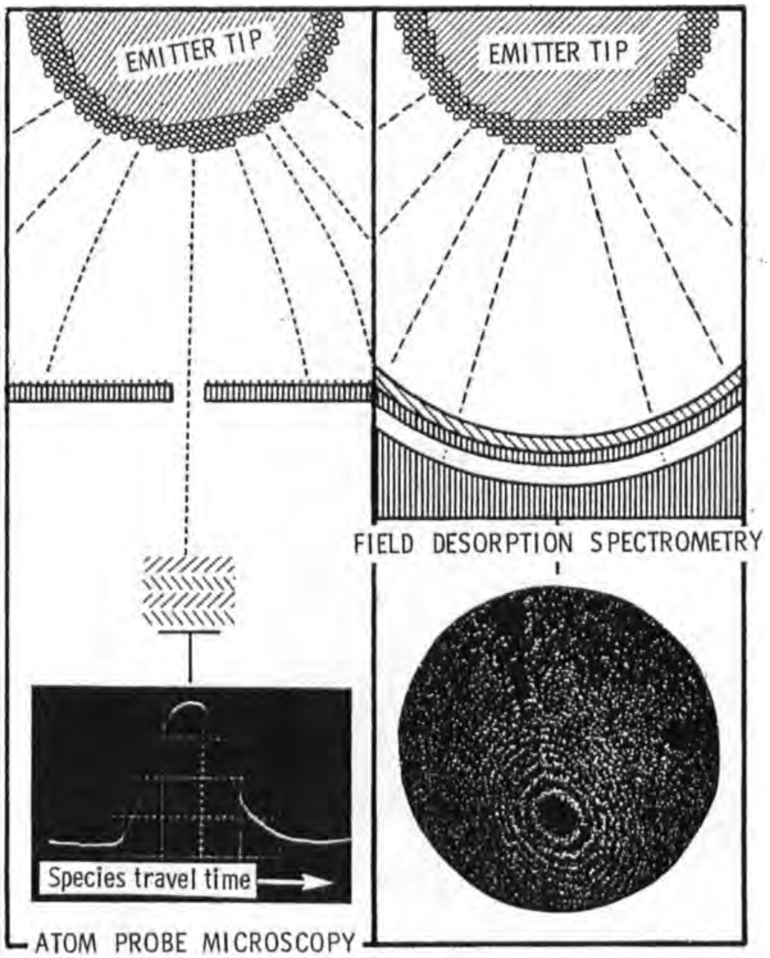

FIGURE 9. Comparison of the atom-probe and imaging field-desorption mass spectrometers. An atom-probe analysis (left) produces a detector signal corresponding to the arrival of one preselected species. A field-desorption analysis (right) gives the complete crystallographic distribution of a preselected species by activating (time-gating) a detector coincidentally with its arrival (see text).

produced by the arrival of one substrate species) is compared to the result of an IFDEMS analysis, showing the crystallographic distribution of that species. Such a distribution is obtained[59] by time-gating the spherical Chevron-CEMA of a 10-cm atom-probe so that it is active only during the arrival of the preselected species (Figure 10). The width of the gating pulse determines the ability of the CEMA to discriminate between the arrival of adjacent species; in other words, it determines the mass resolution of the instrument. A gate pulse 8 ns wide is just barely sufficient to resolve the isotopes of tungsten[60] at specimen potentials below 4 kV. Although it is possible to increase mass resolution by reducing the specimen potential and biasing a counter-electrode[63] to establish the desorption field, the resulting gated image will be displaced with respect to the ion image, making regional comparisons difficult. For compositional profiles, the shift is not a problem, since only species detection is important. However, for adsorption studies attempting to elucidate precise crystallographic behavior, such shifts must be minimized, since only the regularity of the ion image can provide reliable regional identification. It should be noted that the present instrumentation does not permit more than one species' crystallographic distribution to be obtained in an IFDEM experiment during each desorption event. However, this is not a fundamental limitation, since several distributions could be obtained (without gating) by using a nanosecond

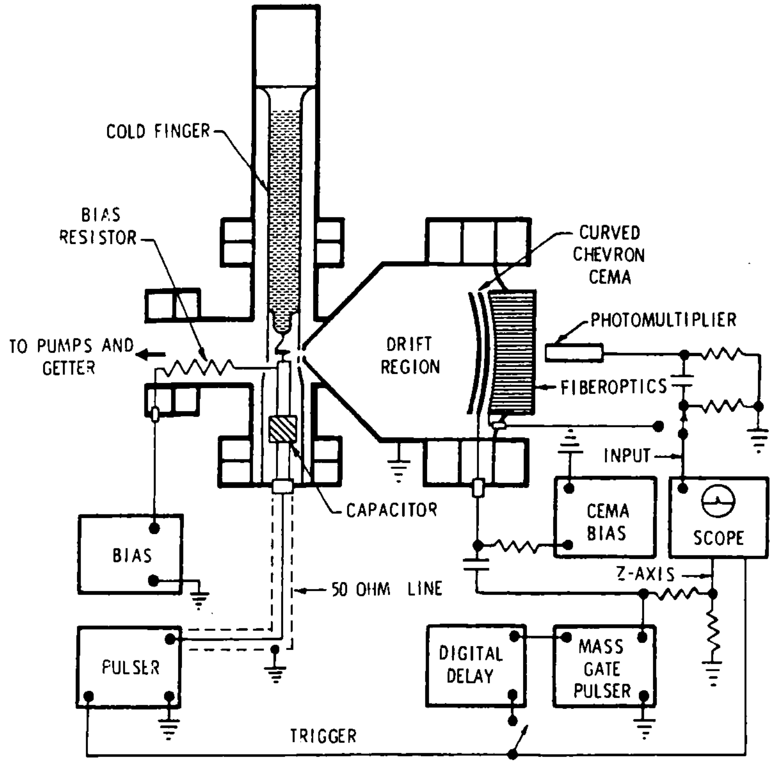

FIGURE 10. The imaging field-desorption mass spectrometer. A 10-cm drift region allows approximately 10% of the desorption image to be recorded on a spherical Chevron CEMA detector. By initiating the sweep of an oscilloscope with the desorption pulse applied to the specimen, the successive arrival of surface species at the CEMA can be recorded as a mass spectrum. A photomultiplier permits localized regional examinations, and a mass gate pulser activating the CEMA coincidently with the arrival of one species permits crystallographic distributions of that species to be obtained.

framing camera to photographically record the successive arrival of each surface species at the CEMA.

Since the ion travel times are short (particularly for the lightest species at the higher specimen potentials), an additional consideration, normally ignored in longer drift-tube instruments, is important. The derivation of Equation 2, used for species identification (or travel-time determination for a given species), ignored the acceleration time of the desorbed species in front of the specimen. If this becomes a nonnegligible fraction of the total travel time, Equation 2 becomes inaccurate and species identification will be affected. If T_0 is the paraxial ion travel time in the acceleration region, it can be shown[101] (to first order) that Equation 2 can be rewritten as follows:

$$\frac{m}{n} \cong \frac{2e}{d^2} V_T (T_{meas})^2 \left[1 - \frac{2T_O}{T_{meas}}\right] \qquad (3)$$

where V_T is the total specimen potential ($V_{DC} + \alpha V_{pulse}$), and T_{meas} is the measured travel time of the paraxial ion. T_0 can be evaluated[13] for a confocal paraboloid geometry by integrating the ion's velocity over the distance, d_0, between the specimen and an "apertureless" counter-electrode (cathode) at ground potential. Then, the ion acceleration correction

$$\Delta \equiv \frac{2T_O}{T_{meas}}$$

can be written,[101] approximately, as

$$\Delta \cong 2G(R/2d_0)\,\frac{d_0}{d} \qquad (4)$$

where G is a slowly varying function of the specimen radius, R, and the acceleration distance, d_0. The quantity d is the usual drift distance

FIGURE 11. Desorption micrograph of tungsten at 78 K taken during continuous DC field evaporation of the substrate and corresponding to the removal of many hundreds of atomic layers. (Micrograph courtesy of Dr. A. J. Moore, CISRO, Australia.)

between cathode and detector. For d_0 = 1 mm, one finds[101]

Δ = 1.8% (d = 0.118 m)

Δ = 0.2% (d = 1 m)

Obviously, the ion acceleration correction is not negligible for short drift distances and must be considered whenever maximum accuracy in species identification is necessary. Although T_0 in Equation 3 was determined specifically for paraxial ions, its value for off-axis ions is only negligibly different,[101] allowing T_0 to be used as the acceleration time of any identical ion, regardless of its emission angle from the specimen. Practically, Δ (Equation 4) does not depend, at least to first order, on the specimen potential, nor on the ion's m/n, nor on its emission angle from the specimen. As a result, the acceleration correction can be treated as a constant in Equation 3, simplifying calibration procedures and subsequent species identification.

XII. FIELD-DESORPTION INVESTIGATIONS

The non-gated field-desorption microscope can provide little quantitative information regarding surface processes, since it cannot mass-analyze the desorbed species. However, a qualitative description of variations in desorbed-ion abundance over the surface (of importance in metallurgical applications) can be obtained. Using slow DC or successive-pulse evaporation to insure removal of many atomic layers of the specimen, remarkably detailed desorption images can be obtained (Figure 11), which show bright regions of high ion abundance and dark regions of low ion yield. Such images were first obtained by Walko and Müller[15] using the desorption microscope.[100] Since many substrate layers are removed during the time the images are recorded, they represent averages over the specific crystallography associated with atom placement in each layer. Waugh, Boyes and Southon[102] have reported similar desorption images for numerous materials; these images were reproducible over a wide range of desorption conditions, indicating that the patterns observed are not due to detector artifacts. Müller and Tsong[15] suggest that dark zone lines in desorption images of platinum probably result from localized ion-optical effects causing a divergence in the trajectories of desorbed species. This explanation has been questioned,[102] and the possibility of short-range atom migration (induced by polarization forces in specific crystallographic directions during the desorption process) has been advanced.[102] Although the mechanisms responsible for the bright and dark zone-line patterns are not understood, it is probable that the dark central regions of major planes in certain desorption studies[15,102,103] are experimental artifacts. In such studies a single CEMA is always used for an ion detector, resulting in poor detection efficiency for the desorbed species. As a result, regions of the surface where the atom density is low and the local curvature is high (resulting in a large ion-trajectory divergence and low image-spot density) will appear dark in the desorption micrograph. If the photographic contrast of the recorded desorption image is high, these regions can appear black or give the impression that no ions were detected. For the close-packed planes, a central dark region must also be considered as an artifact, since other investigators[104,105] have photographically recorded substrate-ion images in the center of the (110) plane of tungsten and in the (111) plane of iridium[106] and platinum[60] during field evaporation.

Time-gating for each of the charge states of the field-evaporating substrate provides further intriguing observations. For tungsten, W^{3+} occurs primarily at the location of protruding surface atoms, producing a characteristic ring pattern in the desorption image that was seen by several authors.[63,100] However, the less abundant species, W^{4+}, seems to originate at almost random locations on the surface,[59] with a slightly higher probability of formation along the (111) zone (Figure 12). Of interest is the increased abundance of W^{4+} during the collapse of the (110) and (211) planes,[60] indicating that the last atoms, evaporating upon removal of a monolayer from the (110) plane, evaporate predominantly as W^{4+}. Such an effect is not observed for iridium, where both Ir^{2+} and Ir^{3+} distributions are similar.[106] However, a noticeable difference in the extent of dark zone-line regions in the gated image of Ir^{2+} and Ir^{3+} is observed. A charge-dependent and crystallographically specific ion-neutralization process might explain this observation,[104] but such a mechanism is difficult to verify, particulary from these preliminary observations.

It is apparent that more work is needed before the mechanisms producing the desorption and the gated desorption patterns are understood. However, the patterns themselves are important, because they show a definite crystallographic variation in ion yield that can depend on the charge state of the evaporated species. Obviously, the phenomenon must be recognized and considered, since it can effect the interpretation of metallurgical studies based on the SAMS technique.

A recent study of noble-gas adsorption on tungsten at 78 K has been described by Panitz[106] who used time-gated desorption micrographs to display He^+ and Ne^+ crystallography. The distributions of helium (Figure 13) and neon on tungsten always reproduce the regions of low ion yield of substrate species, but they may also show additional regions of low image-spot density. Assuming from theoretical considerations[107] that noble-gas adsorption is highly probable for all surface regions, Panitz has argued[106] that these additional regions of low ion yield reflect the formation of stable metal-gas molecular ions, particularly since similar crystallography for WHe^{3+} has been observed in a high-resolution atom-probe study.[92] The presence of highly localized iridium-neon molecular ion formation has been deduced by Panitz[106] on the basis of similar arguments, although high-resolution atom-probe microscopy has not confirmed its presence. Highly localized neide formation on the surface could explain the different abundances of $PdNe^+$ observed when using the TOF and the magnetic atom-probe. In describing the different abundances of $PdNe^+$ observed when using the two instruments,[62] no mention was made of a careful attempt to examine identical regions of the palladium surface.

Hydrogen adsorption on metal surfaces is a particularly interesting system to observe with SAMS, because no other surface-sensitive technique can detect hydrogen directly. Since an ion image cannot reveal the presence of adsorbed hydrogen, and since its variation with surface

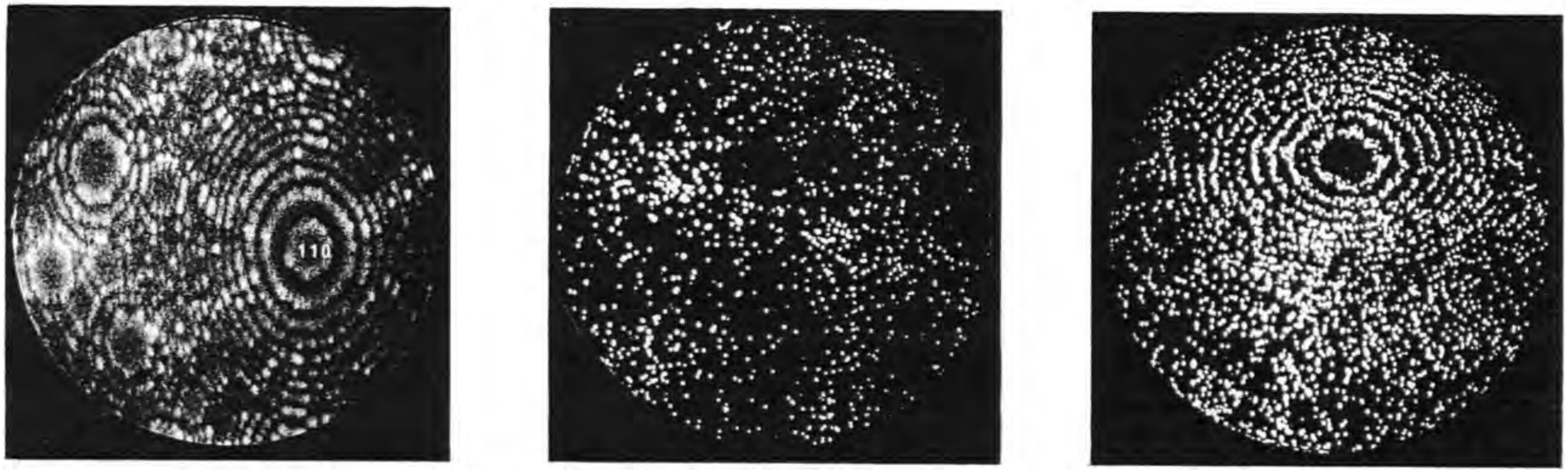

FIGURE 12. Helium-ion image of (110) tungsten (right). Integrated W^{4+} image (middle), 100 desorption events in 100 sec. Integrated W^{3+} image (left), 100 desorption events in 100 sec. $P = 8 \times 10^{-10}$ torr, $T = 78$ K.

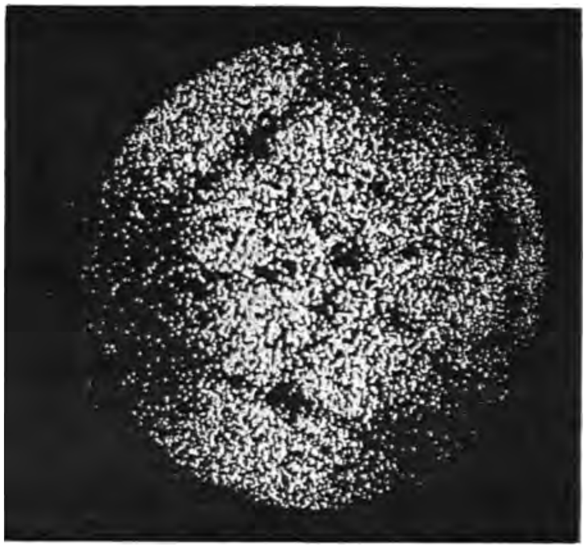

FIGURE 13. Helium (He^+) distribution from tungsten at 78 K. $P_{helium} \leq 3 \times 10^{-10}$ torr. Dark regions reflect regions of low ion yield for substrate species (see text) as well as regions (100, predominantly) where He^+ is not seen. These regions may correspond to areas of high WHe^{3+} yield (see text) or regions where helium field adsorption is negligible.

crystallography is of interest, the use of imaging field-desorption mass spectrometry is suggested. Using this technique, prominent variations in H^+ yield from iridium surfaces have been observed.[108] The morphology of the surface as well as low-field (weak) binding states in the (111) region is reflected in the H^+ distributions. At high fields, when the substrate is field-evaporating, adsorbed hydrogen is observed to originate from relatively open planes, reproducing its ability to probe, by migration, the three-dimensional character of the lattice near the surface. For tungsten, this effect is striking,[108] with the loosely packed planes of the (111) zone prominently displayed, in agreement with Rye's[109] prediction for crystallographic variation in hydrogen adsorption in this region. Unfortunately, the gate-pulse width cannot be reduced sufficiently to resolve substrate hydrides, so that their distribution cannot, now, be determined.

A particularly interesting observation has been the occurrence of highly localized (13 Å) hydrogen-adsorption sites on iridium (Figure 14), associated with a carbon impurity in the lattice.[108] Since two species cannot be observed simultaneously by the present gating technique, the presence of hydrogen at the carbon-impurity sites could only be indirectly determined by alternately gating for carbon and for hydrogen. Because the carbon impurity extended, as clusters of several carbon atoms, in many highly localized regions throughout the lattice, this procedure could be repeated many times, always with identical results. One hydrogen atom was usually observed with each carbon atom in an impurity cluster.

The desorption of hydrogen from a metal can be expected to be a function of both the applied field and the crystallography (the number of binding states varies with crystallographic orientation). As a result, gated desorption experiments are often difficult to interpret. Desorbing at high fields removes all of the hydrogen that binds to the surface at lower fields, producing a desorption image that may include contributions from many separate binding states and crystallographic regions. Desorbing at low fields may remove only a portion of the hydrogen in a single binding state, resulting in a desorption image that is incomplete in that it does not reflect all of the hydrogen in that state. To eliminate these difficulties, another experiment can be performed;[110] a monolayer of hydrogen is adsorbed at zero field, and then the desorption field is linearly ramped (by ramping the specimen potential), with the arrival of all species at the detector recorded as a function of the applied field. Since the dominant desorbing surface species will be hydrogen, variations in desorption current as a function of field will display the character of its binding states in a manner analogous to that provided by thermal-

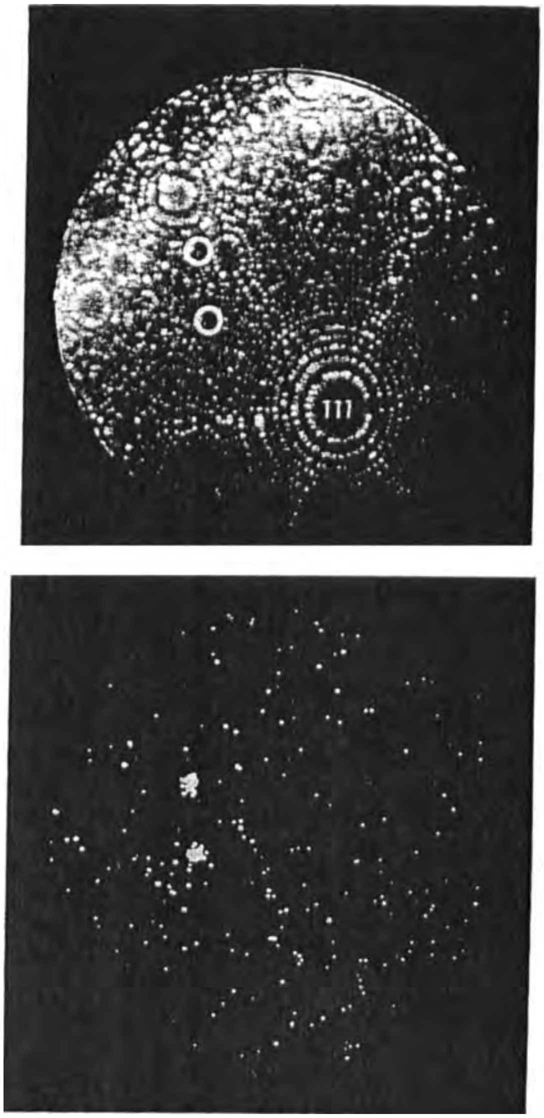

FIGURE 14. (Top) Field-ion image of (111) iridium surface at 78 K. The two white circles denote the position of localized hydrogen adsorption (at a carbon impurity in the lattice). (Bottom) Gated desorption image of H^+ from iridium showing two highly localized regions of hydrogen adsorption. Subsequent gating showed a carbon impurity in the lattice at these locations. Each hydrogen atom was associated with a single carbon atom.

desorption spectra. However, because desorption from many crystallographic regions will be simultaneously detected, the field-desorption spectra will be more complex than their thermal counterparts obtained from single crystal surfaces. To determine the effect of crystal orientation on hydrogen binding, several photomultipliers can be used to identify the desorption current originating from specific regions of the surface. The resulting field-desorption spectra are in close agreement with thermal-desorption spectra on macroscopic single crystals of identical orientation, displaying similiar desorption peaks and reproducing their relative intensities. However, the field-desorption peaks always seem narrower than their thermal counterparts, indicating almost complete thermal accommodation between adsorbate and substrate prior to field desorption. Once the field dependence is established in a particular crystal region, gated desorption images from a specific binding state in the region may reveal[110] the binding site of the adsorbate. Of course, binding sites can only be obtained by comparing a gated desorption micrograph to an ion image, defining the position of the individual substrate atoms prior to adsorption, and then compensating for the effect of trajectory differences between the ion and the desorption images.

XIII. CONCLUSIONS

The single-atom mass spectroscopies have been presented as powerful tools for the investigation of surface-related problems, provided that their limitations are recognized. These limitations result primarily from physical processes induced by high-field desorption, and not from experimental difficulties, which may limit mass resolution or interfere with species identification. Practically, the high electric field at the surface can affect species abundance by promoting the formation of stable complex molecules, by determining a crystallographically dependent variation in ion yield, or by inducing field migration of surface species prior to, or during, the desorption process. Each of these effects must be considered when using the single-atom mass spectroscopies.

It is apparent that the newer gated desorption methods can provide extremely useful information concerning species crystallography, but are limited by low mass resolution. The probe-hole technique can give excellent mass resolution, but it is limited in that species crystallography cannot be obtained during each desorption event. What is needed is a combination of both techniques, obtainable by replacing the screen (or ion-image enhancer) of the atom probe with a gated desorption spectrometer. In this way, species crystallography obtained with the latter can be used as a guide for high (mass) resolution, probe-hole analysis of specific regions of interest. Practically, time-gating the usual CEMA ion-image enhancer of most current atom probes will provide this useful capability with minimal effort. Such a feature would make maximum use of the great surface-sensitivity of both techniques while providing a greater capability than available with either technique alone.

ACKNOWLEDGMENTS

The author wishes to thank R. J. Walko and R. R. Rye of Sandia Laboratories for a critical reading of this manuscript. The author's research was supported by the United States Energy Research and Development Administration.

REFERENCES

1. **Müller, E. W.,** *Z. Phys.,* 131, 136, 1951.
2. **Müller, E. W.,** *Phys. Rev.,* 102, 618, 1956.
3. *Field evaporation* refers to the high-field process by which lattice atoms are removed from the specimen as positive ions. *Field desorption* is a more general term, referring to the field-induced removal of any substrate species.
4. **Boudart, M.,** The R. A. Welch Foundation Conference on Chemical Research. XIV. Solid State Chemistry, Ch. VII, Houston, Texas, 1970, 300.
5. **Drechsler, M.,** *Z. Elektrochem.,* 61, 48, 1957.
6. **Tsong, T. T. and Walko, R. J.,** *Phys. Status Solidi A,* 12, 111, 1972.
7. **Graham, W. R. and Ehrlich, G.,** *Surf. Sci.,* 45, 544, 1974.

8. Muller, E. W. and Panitz, J. A., 14th Field Emission Symposium, Washington, D.C., 1967.
9. Inghram, M. G. and Gomer, R., *J. Chem. Phys.*, 22, 1297, 1954.
10. Beckey, H. D., *Field Ionization Mass Spectroscopy*, Pergamon Press, New York, 1970.
11. Barofsky, D. F. and Muller, E. W., *Surf. Sci.*, 10, 177, 1968.
12. Müller, E. W., Panitz, J. A., and McLane, S. B., *Rev. Sci. Instrum.*, 39, 83, 1968.
13. Panitz, J. A., Ph.D. Dissertation, The Pennsylvania State University, 1969.
14. Suvorov, A. L. and Trebukhovskii, V. V., *Sov. Phys.*, 15(4), 471, 1973.
15. Muller, E. W. and Tsong, T. T., *Progress in Surface Science*, Vol. 4, Part 1, Pergamon New York, 1973.
16. Muller, E. W., *J. Microsc.* (Oxford), 100(2), 121, 1974.
17. Muller, E. W., *Jap. J. Appl. Phys.*, Suppl. 2, Pt. 2, 1, 1974.
18. Brenner, S. S. and McKinney, J. T., *Surf. Sci.*, 23, 88, 1970.
19. Mikhailovskii, I. M., Eres'ko, A. P., and Kul'ko, V. B., *Sov. Instrum. Exp. Tech.*, 16, 612, 1973.
20. Block, J. H., *Vac. Tech.*, 22, 190, 1974.
21. Nakamura, S., *Jap. J. Vac. Soc.*, 7, 228, 1974.
22. Hall, T. M., Wagner, A., Berger, A. S., and Seidman, D. N., Cornell University Materials Science Center Report #2357, 1975.
23. Hochman, R. F., Müller, E. W., and Ralph, B., Eds., *Applications of Field Ion Microscopy in Physical Metallurgy and Corrosion*, Georgia Institute of Technology, Atlanta, 1969.
24. Muller, E. W., McLane, S. B., and Panitz, J. A., 4th European Conference on Electron Microscopy, Rome, Italy, 1968, 135.
25. Turner, P. J., Regan, B. J., and Southon, M. J., *Vacuum*, 22, 443, 1972.
26. Stoltz, D. L., Ph.D. thesis, University of Florida, 1972.
27. Müller, E. W., *Ber. Bunsenges.*, 75, 979, 1971.
28. Müller, E. W., *Naturwissenschaften*, 57, 222, 1970.
29. Regan, B. J., Pate, C. L., Boyes, E. D., and Southon, M. J., 19th Field Emission Symposium, Urbana, Ill., 1972.
30. Muller, E. W., and Tsong, T. T., *Field Ion Microscopy, Principles and Applications*, Elsevier, New York, 1969, 133.
31. Turner, P. J. and Southon, M. J., in *Dynamic Mass Spectroscopy*, Vol. 1, Price, D., and Williams, J. E., Eds., Heyden & Son, London, 1970.
32. Brenner, S. S. and McKinney, J. T., *Rev. Sci. Instrum.*, 43, 1264, 1972.
33. Müller, E. W., Krishnaswamy, S. V., and McLane, S. B., *Rev. Sci. Instrum.*, 44, 84, 1973.
34. Johnson, C. A., *Rev. Sci. Instrum.*, 41, 1812, 1970.
35. Berger, A. S., *Rev. Sci. Instrum.*, 44, 592, 1973.
36. McLane, S. B., 20th Field Emission Symposium, University Park, Pa., 1973.
37. Panitz, J. A., McLane, S. B., and Muller, E. W., *Rev. Sci. Instrum.*, 40, 1321, 1969.
38. Wagner, A., Hall, T. M., and Seidman, D. N., Cornell University Material Science Center Report #2392, 1975; *Rev. Sci. Instrum.*, August 1975.
39. Panitz, J. A., Sandia Laboratory Report SAND75-0116, 1975.
40. Ehrlich, G., in *Interatomic Potentials and Simulation of Lattice Defects*, Genlen, P. C., Beeler, J. R., and Jaffee, R. I., Eds., Plenum Press, New York, 1972.
41. Lucas, A. A., *Phys. Rev., Lett.*, 26, 813, 1971.
42. Lucas, A. A. and Sunjic, M., *J. Vac. Sci. Technol.*, 9, 725, 1972.
43. Müller, E. W., *Lab. Prac.*, 22, 408, 1973.
44. Krishnaswamy, S. V. and Muller, E. W., 20th Field Emission Symposium, University Park, Pa., 1973.
45. Lewis, R. J. and Smith, G. D. W., 20th Field Emission Symposium University Park, Pa., 1973.
46. Krishnaswamy, S. V. and Müller, E. W., *Rev. Sci. Instrum.*, 45, 1049, 1974.
47. Regan, P. J., Turner, P. J., and Southon, M. J., to be published.
48. Müller, E. W. and Krishnaswamy, S. V., *Rev. Sci. Instrum.*, 45, 1053, 1974.
49. Poschenrieder, W. P., *Int. J. Mass Spectrom. Ion Phys.*, 9, 357, 1972.
50. Müller, E. W., private communication.
51. Defined as the mass peak width at half maximum.
52. Seidman, D. N., private communication.
53. Muller, E. W., 13th Field Emission Symposium, Bonn, Germany, 1968.
54. Panitz, J. A., 20th National Symposium, American Vacuum Society, New York, 1973.
55. Galileo Electro-optics, Sturbridge, Mass.
56. Burroughs, E. G., *Rev. Sci. Instrum.*, 40, 35, 1969.
57. Panitz, J. A. and Foesch, J. E., to be published.
58. Panitz, J. A., unpublished data, 1973.
59. Panitz, J. A., *J. Vac. Sci. Technol.*, 11, 206, 1974.
60. Panitz, J. A., unpublished data, 1974.
61. Schulten, H. R. and Schurath, U., *J. Chem. Phys.*, 79, 51, 1975.
62. Müller, E. W. and Sakurai, T., *J. Vac. Sci. Technol.*, 11, 878, 1974.
63. Panitz, J. A., *Rev. Sci. Instrum.*, 44, 1034, 1973.

64. Müller, E. W. and Walko, R. J., 19th Field Emission Symposium, Urbana, Ill., 1972.
65. Müller, E. W. and Nishikawa, O., Technical Publication N431, American Society for Testing and Materials, Philadelphia, 1968.
66. Walko, R. J., Ph.D. dissertation, The Pennsylvania State University, 1974.
67. Musket, R. J., Special Course on Surface Analysis, American Vacuum Society, Anaheim, Calif., 1974.
68. Brenner, S. S. and Goodman, S. R., *Scr. Metall.*, 5, 865, 1971.
69. Goodman, S. R., Brenner, S. S., and Low, J. R., Jr., *Metall. Trans.*, 4, 2371, 1973.
70. Youle, A., Turner, P. J., and Ralph, B., *J. Microsc.*, 101, 1, 1973.
71. Turner, P. J. and Papazian, M. J., *Met. Sci.*, 7, 81, 1973.
72. Turner, P. J., Regan, B. J., and Southon, M. J., *Surf. Sci.*, 35, 336, 1973.
73. Dunlop, G. L. and Turner, P. J., to be published.
74. Krishnaswamy, S. V., McLane, S. B., and Müller, E. W., *J. Vac. Sci. Technol.*, 11, 899, 1974.
75. Park, R. L., Houston, J. E., and Schreiner, D. G., *J. Vac. Sci. Technol.*, 9, 1023, 1972.
76. Brenner, S. S. and Goodman, S. R., *Nat. Phys. Sci.*, 234, 35, 1972.
77. Easterfield, J. and Linnet, J. W., *Nature*, 226, 143, 1970.
78. Tsong, T. T., Krishnaswamy, S. V., McLane, S. B., and Müller, E. W., *Appl. Phys. Lett.*, 23, 1, 1973.
79. Tsong, T. T. and Müller, E. W., *J. Appl. Phys.*, 45, 2367, 1974.
80. Southworth, H. N., *J. Appl. Phys.*, 45, 2364, 1974.
81. Jason, A. J., *Phys. Rev.*, 156, 266, 1967.
82. Utsumi, T. and Smith, N. V., *Phys. Rev. Lett.*, 33, 1294, 1974.
83. Fonash, S. J. and Schrenk, G. L., *Phys. Rev.*, 180, 649, 1969.
84. Brenner, S. S. and McKinney, J. T., *Appl. Phys. Lett.*, 13, 29, 1968.
85. Müller, E. W., *Q. Rev. Chem. Soc.* (London), 23, 177, 1969.
86. Müller, E. W., McLane, S. B., and Panitz, J. A., *Surf. Sci.*, 17, 430, 1969.
87. McKinney, J. T. and Brenner, S. S., 16th Field Emission Symposium, Pittsburgh, Pa., 1969.
88. Tsong, T. T. and Müller, E. W., *Phys. Rev. Lett.*, 25, 911, 1970.
89. Müller, E. W. and Krishnaswamy, S. V., *Surf. Sci.*, 36, 29, 1973.
90. Nolan, D. N. and Herman, R. M., *Phys. Rev.*, B8, 4099, 1973.
91. Müller, E. W., Krishnaswamy, S. V., and McLane, S. B., *Surf. Sci.*, 23, 112, 1970.
92. Müller, E. W., Krishnaswamy, S. V., and McLane, S. B., *Phys. Rev. Lett.*, 31, 1282, 1973.
93. Sakurai, T., Tsong, T. T., and Müller, E. W., *Phys. Rev.*, B10, 4205, 1974.
94. Brenner, S. S. and McKinney, J. T., *Surf. Sci.*, 20, 411, 1970.
95. Panitz, J. A., 33rd Physical Electronics Conference, Berkeley, Calif., 1973.
96. Müller, E. W., Krishnaswamy, S. V., and McLane, S. B., 32nd Physical Electronics Conference, Washington, D.C., 1971.
97. Mulson, J. F. and Müller, E. W., *J. Chem. Phys.*, 38, 2615, 1963.
98. Müller, E. W. and Bahadur, K., *Phys. Rev.*, 102, 624, 1956.
99. George, T. H., *Bull. Am. Phys. Soc.*, 10, 493, 1965.
100. Walko, R. J. and Müller, E. W., *Phys. Status Solidi A*, 9, K9, 1972.
101. Panitz, J. A., Sandia Laboratory Report SAND75-0117, 1975.
102. Waugh, A. R., Boyes, E. D., and Southon, M. J., *Nature*, 253, 342, 1975.
103. Moore, A. J. and Spink, J. A., 21st Field Emission Symposium, Marseille, France, 1974.
104. Panitz, J. A., 21st Field Emission Symposium, Marseille, France, 1974.
105. Walko, R. J., private communication.
106. Panitz, J. A., *J. Vac. Sci. Technol.*, 12, 210, 1975.
107. Tsong, T. T. and Müller, E. W., *J. Chem. Phys.*, 55, 2884, 1971.
108. Panitz, J. A., Proceedings of The Hydrogen Economy Miami Energy (THEME) Conference, Miami Beach, Florida, 1974, S6-33.
109. Rye, R. R., Barford, B. D., and Cartier, P. G., *J. Chem. Phys.*, 59, 1693, 1973.
110. Panitz, J. A., to be published.